

## Electron Holography Surmounts Resolution Limit of Electron Microscopy

A. Orchowski, W. D. Rau, and H. Lichte

*Institut für Angewandte Physik der Universität Tübingen, D-72076 Tübingen, Germany*

(Received 8 August 1994)

In high resolution electron off-axis holography, the complete information about amplitude and phase of the complex electron image wave is captured in a single hologram, fed to a computer, numerically reconstructed, and analyzed using methods of wave optical image processing. Specifically, the blurring effect due to the aberration of the objective lens of the electron microscope is corrected under reconstruction. The presented first results, achieved with a Philips CM30FEG electron microscope specially developed for the needs of high resolution electron holography, reveal that the point resolution of modern electron microscopes is significantly improved.

PACS numbers: 61.16.-d, 42.30.Rx, 42.40.-i

In contrast to the light optical case, in electron microscopy the lateral resolution is not limited by the diffraction error, i.e., by the wavelength of the electrons, but instead is governed by the spherical aberration of the objective lens. As shown by Scherzer [1] already in 1936, this error cannot be avoided as long as common rotational symmetric lens designs are used. For example, in the case of the Philips CM30FEG high resolution electron microscope applied in this work, the best point resolution is 0.198 nm, about 2 orders of magnitude worse than the diffraction limit of the  $\lambda = 1.98$  pm wavelength, 300 keV electrons.

In electron microscopy we deal with a complex electron wave  $o(\mathbf{r}) = a(\mathbf{r}) \exp[i\varphi(\mathbf{r})]$  modulated in both amplitude and phase due to the interaction with the object. During the imaging process from this object wave to the recordable image wave, the aberrations of the objective lens lead to a blurring of the available information. The backpropagation from the aberration-corrupted image wave  $b(\mathbf{r}) = A(\mathbf{r}) \exp[i\Phi(\mathbf{r})]$  to the level of the object is possible following the wave laws given by the Kirchhoff diffraction integral. Prerequisites are the registration of the image wave amplitude and phase as well as a sufficient knowledge of the lens aberrations. This approach—called holography—was proposed by Gabor already in 1948 [2] but it took nearly 50 years until electron holography finally achieved this goal.

From the various forms of electron holography [3] under investigation, the off-axis technique has proven to be most promising [4]. Using a Moellenstedt biprism, the image wave is coherently superimposed with a plane reference wave, and the resulting interference pattern—the hologram—reveals a cosinusoidal intensity distribution,

$$I(\mathbf{r}) = 1 + A(\mathbf{r})^2 + 2A(\mathbf{r}) \cos(2\pi\mathbf{q}_c \cdot \mathbf{r} + \Phi(\mathbf{r})). \quad (1)$$

Amplitude  $A$  and phase  $\Phi$  of the image wave are captured as a contrast modulation and a bending of the hologram fringes, respectively. The spacing of the hologram fringes  $1/q_c$  can be adjusted by the tilt angle between the image and reference waves. In addition to the cosinusoidal fringes, a conventional high resolution image is found in

the hologram represented as the squared amplitude of the image wave  $A(\mathbf{r})^2$  (Fig. 3). Since the hologram fringes act as carrier wave for amplitude and phase, the image wave can numerically be extracted from the hologram using an according separation technique in Fourier space (see, e.g., [4]). The reconstructed image wave still is distorted by the aberrations of the electron microscope. The description is best performed in Fourier space, where the complex image wave spectrum is given as

$$B(\mathbf{q}) = O(\mathbf{q}) \exp[-i\chi(\mathbf{q})] E_s(\mathbf{q}, D_z) E_c(\mathbf{q}). \quad (2)$$

The different frequency components  $\mathbf{q}$  of the object wave spectrum  $O(\mathbf{q})$  are shifted differently in phase by the wave aberration  $\chi(\mathbf{q})$  which is—in the rotationally symmetric case—given by

$$\chi(\mathbf{q}) = \frac{2\pi}{\lambda} \left[ \frac{1}{4} C_s \lambda^4 q^4 + \frac{1}{2} D_z \lambda^2 q^2 \right], \quad (3)$$

with defocus  $D_z$  and coefficient of spherical aberration  $C_s$ . This representation implies isoplanacy, i.e., independence of the aberrations from the image coordinates. Restriction of spatial and temporal coherence occurring even with modern highly coherent field emission guns leads to a damping of high resolution information by the envelope functions of spatial coherence  $E_s(\mathbf{q}, D_z)$  and chromatic aberration  $E_c(\mathbf{q})$ . The spatial frequency at which damping below noise level occurs represents the “information limit” beyond which no object information is found, neither in a conventional image nor in a hologram.

Mainly because the effective phase plate  $\chi(\mathbf{q})$  is a strongly varying function of spatial frequency, object and image wave usually do not agree. The upper part of Fig. 1 shows the  $\sin\chi$  function that is responsible for the transfer of the object wave phase into the image wave amplitude (the square of which only can be recorded in conventional microscopy) in the so-called “Scherzer condition.” This condition is conventionally used in high resolution microscopy, when the “weak phase object approximation” applies, since a broad range of spatial frequencies is transferred with the ideal “Zernike phase shift” of  $\chi(\mathbf{q}) = -\pi/2$  well known from light optics

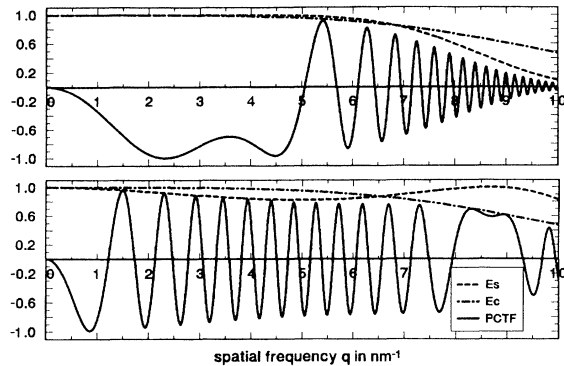


FIG. 1. Phase contrast transfer function (PCTF)  $\sin \chi$  of CM30FEG electron microscope with Supertwin lens ( $C_s = 1.2$  mm,  $U_b = 300$  kV) at Scherzer defocus ( $D_z = -59.5$  nm, top) and at optimum focus ( $D_z^{\text{opt}} = -348$  nm, bottom) for correction up to  $10 \text{ nm}^{-1}$ . For damping functions, energy width  $\Delta E = 1$  eV, coefficient of chromatic aberration  $C_c = 1.4$  nm, and illumination aperture of  $0.1$  mrad was assumed. Note that at optimum focus the damping of the high spatial frequencies is much more favorable.

[4,5]. The definition of the so-called ‘‘Scherzer resolution limit’’ as the first zero crossing of the  $\sin \chi$  function under this condition becomes obvious: higher spatial frequencies are transferred with increasingly rapid oscillations in contrast so that a direct interpretation of the corresponding fine image details in terms of object structure is no longer possible [6]. In conventional microscopy, these spatial frequency components are therefore often filtered out. On the other hand, holography can make full use of all spatial frequencies thus pushing the resolution limit to the information limit.

Since in electron holography amplitude and phase of the image wave are available, a numerical phase plate inverse to  $\chi(\mathbf{q})$  can be applied in Fourier space to remove the coherent aberrations [7]. Then the oscillations of the transfer functions  $\sin \chi$  and  $\cos \chi$  are removed, hence the application of the Scherzer condition in holography is no longer necessary. Instead, a different focus is preferable, optimizing damping envelopes and sampling of the transfer function for subsequent correction of aberrations. For a desirable resolution of  $1/q_{\text{max}}$  well inside the information limit, the hologram preferably is recorded at the defocus

$$D_z^{\text{opt}} = -0.75 C_s (q_{\text{max}}/k)^2, \quad (4)$$

where  $k$  represents the wave number  $1/\lambda$  [8]. Then, by correction of aberrations an improvement in resolution with respect to the Scherzer resolution limit  $q_s$  of

$$\frac{q_{\text{max}}}{q_s} = 0.3 N_{\text{pix}}^{1/4} \quad (5)$$

can theoretically be achieved, where  $N_{\text{pix}} \times N_{\text{pix}}$  denotes the input pixel capacity of the detector used. The limitation imposed by the limited number of pixels used for digitizing the holograms is due to the necessary

reconstruction procedure: only a fraction of the input pixel capacity [approximately  $(N_{\text{pix}}/6)^2$ ] is available to represent the reconstructed wave and therefore sampling problems in the numerical modeling of the transfer function arise even under optimum conditions [9].

The Philips CM30FEG–Special Tübingen electron microscope that incorporates special features for the needs of atomic resolution off-axis holography shows a Scherzer resolution limit of  $0.198$  nm (Fig. 1); also the  $\sin \chi$  function at the optimum focus for a correction of aberrations up to a resolution of  $q_{\text{max}} = 10 \text{ nm}^{-1}$  is shown. Diffractometric measurements confirmed an information limit of  $0.1$  nm [10]. For the digitization of the holograms a specially developed electron image detector based on a slow scan charge coupled device (CCD) camera with  $1024 \times 1024$  pixels is used that was optimized for the detection of  $300$  keV electron images [11]. In combination with a fast image processing system of TIETZ Company (Munich), the holographic reconstruction and aberration correction procedure can be performed on-line at the electron microscope within several seconds. Using this instrumental setup, a maximum resolution of  $0.12$  nm can be expected after correction of aberrations; this limit is mainly set by undersampling the aberration function for higher spatial frequencies due to the limited pixel number of the camera system [Eq. (5)] [12,13].

The characteristic ‘‘dumbbell’’ contrast of the tetrahedral Si structure in [110] projection (spacing  $0.136$  nm) is commonly used as a test object in high resolution electron microscopy. Figure 2 shows the schematic arrangement of the atom columns and a simulated image where all beams up to a spacing of  $0.13$  nm have been assumed to pass the objective aperture [14]; the  $\{004\}$  beams (Fig. 2, right) have to contribute to the image formation process, if the structure is to be properly resolved [15]. Because of the influence of spherical aberration and defocus, the dumbbell structure is not resolved. Figure 3 shows a hologram of Si in [110] orientation taken at the CM30FEG. At a hologram fringe spacing of  $0.05$  nm, the complete sideband used for reconstructing the image wave is clearly separated from the center band, which represents the power spectrum of the conventional high

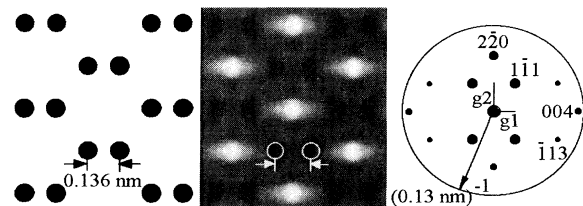


FIG. 2. Left: [110] projection of tetrahedral Si structure produces a characteristic dumbbell-like arrangement of atom columns. Middle: image simulated for an objective aperture of  $0.13 \text{ nm}^{-1}$ , a defocus of  $-60$  nm, and data of the CM30FEG (object thickness  $6.1$  nm). Right: Diffraction pattern of simulated wave;  $\{002\}$  reflections are kinematically forbidden.

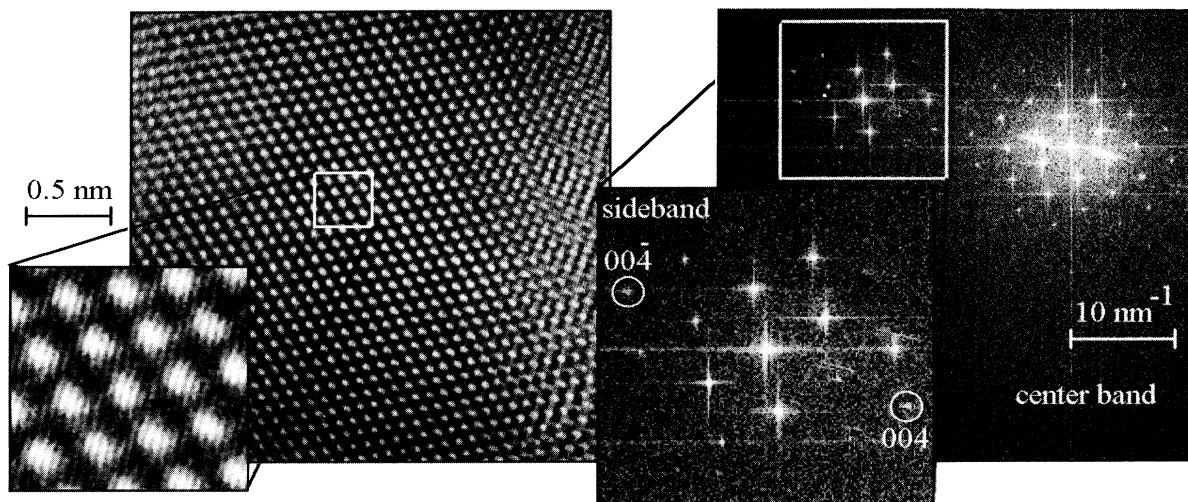


FIG. 3. Hologram of Si [110] taken at the CM30FEG. The spacing of the hologram fringes amounts to 0.05 nm. The Fourier spectrum of the hologram reveals that the sideband used for the holographic reconstruction contains the  $\{111\}$ ,  $\{220\}$ ,  $\{113\}$ , and  $\{004\}$  reflections corresponding to lateral information of 0.136 nm.

resolution image. The  $\{004\}$  reflections are available for reconstruction. Amplitude and phase of the aberration corrected object wave are shown in Fig. 4: Because of the correction, the information previously spread out in the intensity distribution of the hologram is reconcentrated at the atom columns. The white dumbbell contrast in the phase image, that directly represents the atom positions, becomes visible and the amplitude image shows a dark “figure-eight”-shaped contrast with faint white dots at the atom columns; for a better visualization, some noise reduction (Fourier filtering of the nonperiodic background in the spectrum) has been applied [16]. To confirm the proper correction, a simulated thickness-defocus tableau

for  $C_s = 0$  and a residual error in defocus correction in the range of  $-10$  to  $10$  nm has been calculated for different object thicknesses (Fig. 5). It reveals that already small deviations of about 5 nm in defocus drastically change the image contrast of amplitude and phase. Comparing the corrected object wave amplitude and phase from Fig. 4 with the correction tableau reveals a satisfying agreement with the simulations [17]. The asymmetry visible in amplitude and phase of the corrected wave as well as in the corresponding spectrum suggests a residual crystal or beam tilt, revealing that electron holography is a valuable tool for the analysis of such effects: investigations based on comparison with simulations are in progress.

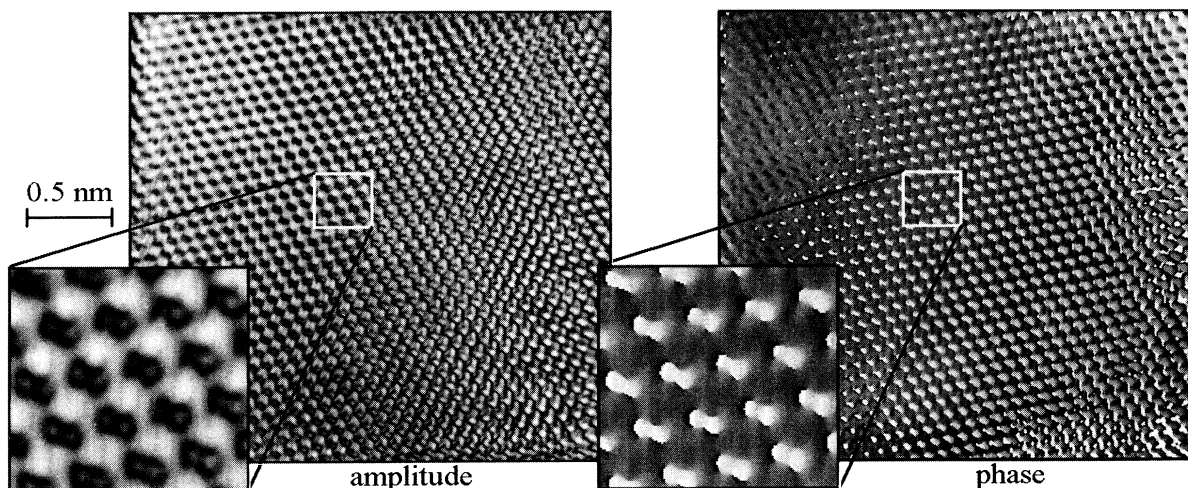


FIG. 4. Aberration-corrected amplitude and phase of electron object wave reconstructed from Fig. 1. (Parameters:  $C_s = 1.23$  mm,  $D_z = -115$  nm,  $C_a = -3$  nm, and  $\phi_a = 120^\circ$ .) The deviation from optimum focus is not severe in this case, because the phase plate used for correction is properly sampled up to the desired frequency. Because of correction, the characteristic Si-dumbbell structure is clearly visible.

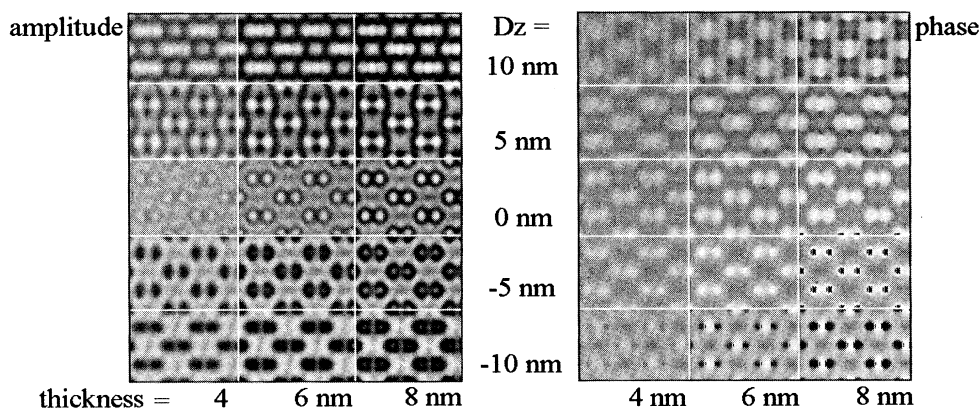


FIG. 5. Simulated thickness-defocus tableau of Si [110] for a correction to  $C_s = 0$ . The comparison with the experimentally reconstructed object wave from Fig. 4 reveals a satisfactory agreement with the simulation for  $D_z = 0$ .

Using the wave optical backpropagation to the level of the object wave, the off-axis holographic technique therefore shows it to be able to retrieve interpretable information from the domain far below the Scherzer resolution limit. Following Eq. (5), the full use of the information down to 0.1 nm, as it is given by the CM30FEG, can only be made when CCD detector systems with  $2048 \times 2048$  pixels are applied for the detection of the holograms; such camera systems are now commercially available. Meanwhile, Fig. 6 demonstrates the capability to record the according information at the example of the image wave spectrum obtained from a Si [110] hologram: The maximum resolution in the sideband is represented by the included  $1\bar{1}5$  reflection that corresponds to a lateral spacing of 0.104 nm.

Thanks are due to the BRITE/EURAM partners, especially to Professor Dirk van Dyck and Dr. Wim Coene

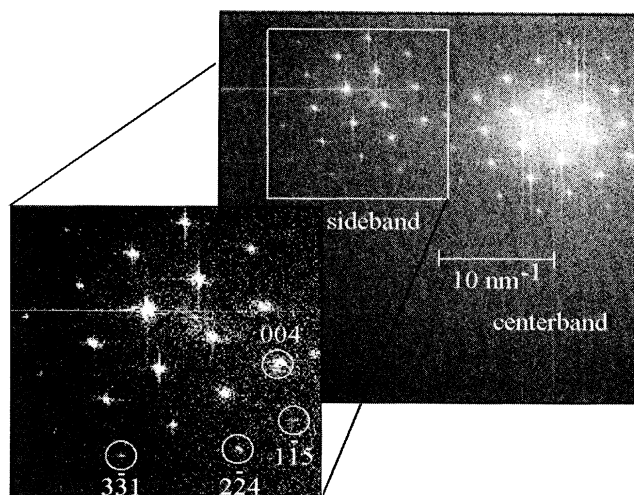


FIG. 6. Spectrum of image wave reconstructed from a Si [110] hologram containing information up to 0.104 nm. The  $3\bar{3}1$ ,  $2\bar{2}4$ , and  $1\bar{1}5$  reflections present correspond to lateral information of 0.124, 0.111, and 0.104 nm, respectively.

for many valuable discussions. Furthermore, the help and profound experience contributed by Professor K.H. Herrmann, Dr. I. Daberkow, and Dr. L. Liu for building up the CCD detector is highly appreciated. Additional thanks go to Alexander Harscher for preparing the specimen. The support of this work by the Körber Stiftung, Hamburg, the Volkswagenstiftung, the Deutsche Forschungsgemeinschaft, and the European Community (BRITE/EURAM) is gratefully acknowledged.

- [1] O. Scherzer, *Z. Phys.* **101**, 593 (1936).
- [2] D. Gabor, *Nature (London)* **161**, 777 (1948).
- [3] J. M. Cowley, *Ultramicroscopy* **41**, 335 (1992).
- [4] H. Lichte, in *Electron Image Plane Off-Axis Holography of Atomic Structures*, edited by T. Mulvey and C.J.R. Sheppard, *Advances in Optical and Electron Microscopy* Vol. 12 (Academic Press, New York, 1991), p. 25.
- [5] J.C.H. Spence, *High Resolution Electron Microscopy* (Oxford University Press, New York, 1988).
- [6] M. A. O'Keefe, *Ultramicroscopy* **47**, 282 (1992).
- [7] Q. Fu, H. Lichte, and E. Völkl, *Phys. Rev. Lett.* **67**, 2319 (1991).
- [8] H. Lichte, *Ultramicroscopy* **38**, 13 (1991).
- [9] H. Lichte, *Ultramicroscopy* **51**, 15 (1993).
- [10] H. Lichte, P. Kessler, F. Lenz, and W.D. Rau, *Ultramicroscopy* **52**, 575 (1993).
- [11] I. Daberkow, K.H. Herrmann, L. Liu, and W.D. Rau, *Ultramicroscopy* **38**, 215 (1991).
- [12] W.D. Rau, H. Lichte, E. Völkl, and U. Weierstall, *J. Comp. Ass. Microscopy* **3**, 51 (1991).
- [13] W.D. Rau, *MSA Bull.* **24**, 459 (1994).
- [14] P. Stadelmann, *Ultramicroscopy* **21**, 131 (1987).
- [15] R. W. Glaisher, A. E. C. Spargo, and D. J. Smith, *Ultramicroscopy* **27**, 19 (1989).
- [16] H. Lichte and W.D. Rau, *Ultramicroscopy* (to be published).
- [17] A. Orchowski, W.D. Rau, and H. Lichte, in *Proceedings of the International Congress on Electron Microscopy, Paris, 1994* (unpublished), p. 297.

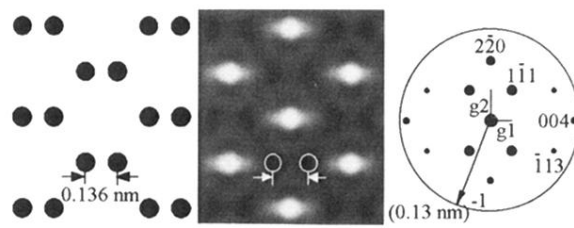


FIG. 2. Left: [110] projection of tetrahedral Si structure produces a characteristic dumbbell-like arrangement of atom columns. Middle: image simulated for an objective aperture of  $0.13 \text{ nm}^{-1}$ , a defocus of  $-60 \text{ nm}$ , and data of the CM30FEG (object thickness  $6.1 \text{ nm}$ ). Right: Diffraction pattern of simulated wave;  $\{002\}$  reflections are kinematically forbidden.

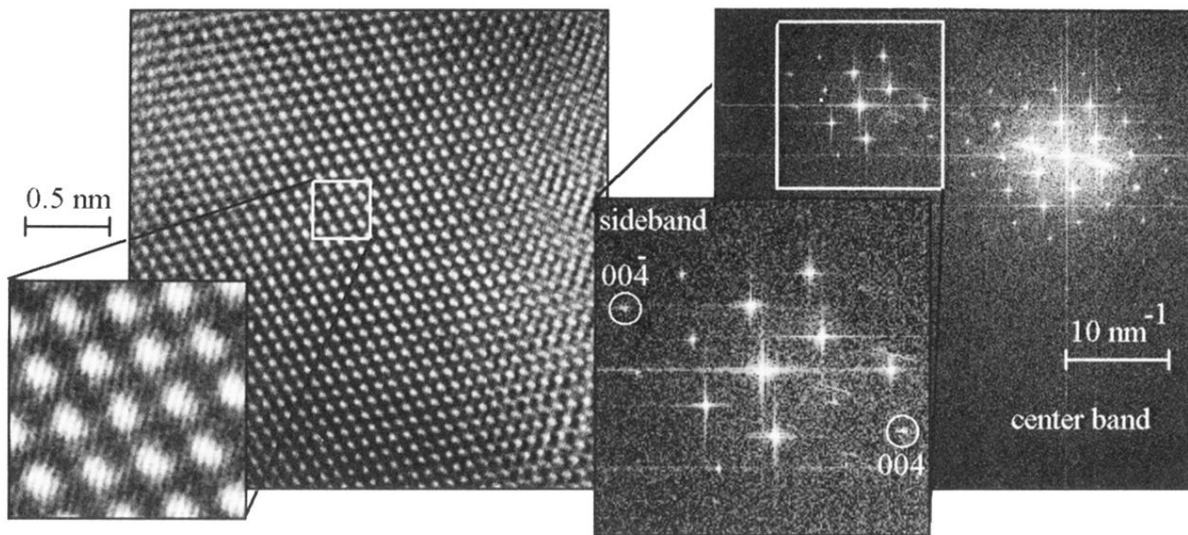


FIG. 3. Hologram of Si [110] taken at the CM30FEG. The spacing of the hologram fringes amounts to 0.05 nm. The Fourier spectrum of the hologram reveals that the sideband used for the holographic reconstruction contains the {111}, {220}, {113}, and {004} reflections corresponding to lateral information of 0.136 nm.

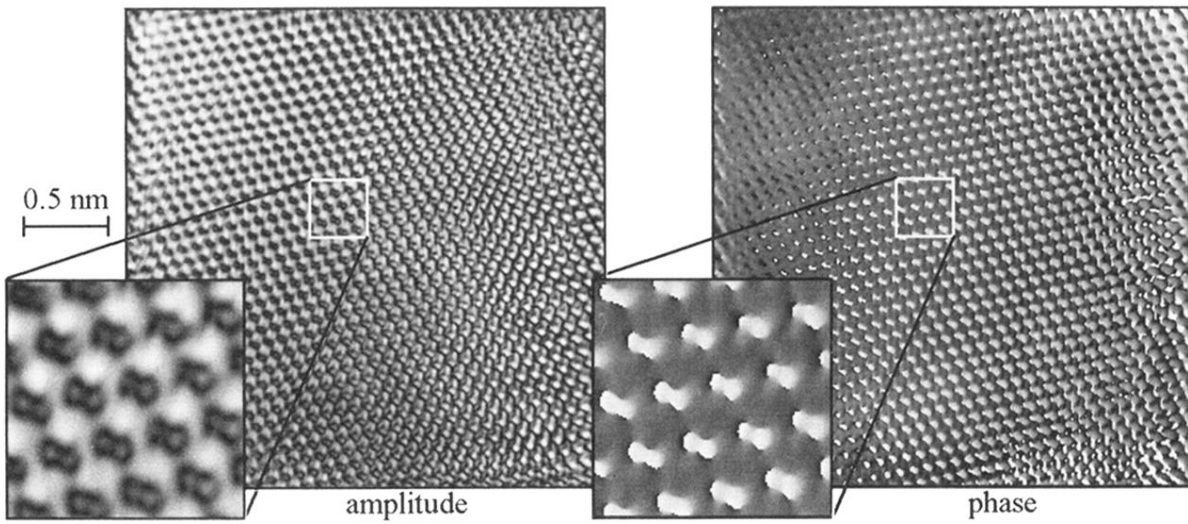


FIG. 4. Aberration-corrected amplitude and phase of electron object wave reconstructed from Fig. 1. (Parameters:  $C_s = 1.23$  mm,  $D_z = -115$  nm,  $C_a = -3$  nm, and  $\phi_a = 120^\circ$ .) The deviation from optimum focus is not severe in this case, because the phase plate used for correction is properly sampled up to the desired frequency. Because of correction, the characteristic Si-dumbbell structure is clearly visible.

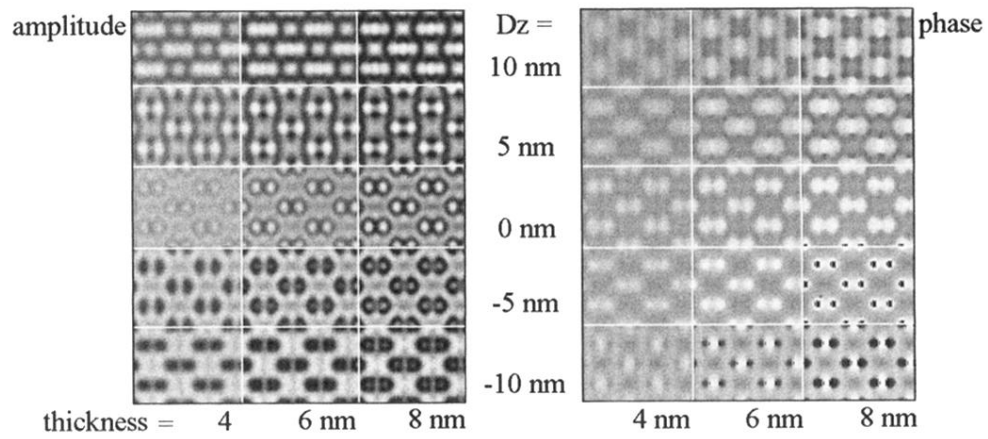


FIG. 5. Simulated thickness-defocus tableau of Si [110] for a correction to  $C_s = 0$ . The comparison with the experimentally reconstructed object wave from Fig. 4 reveals a satisfactory agreement with the simulation for  $D_z = 0$ .

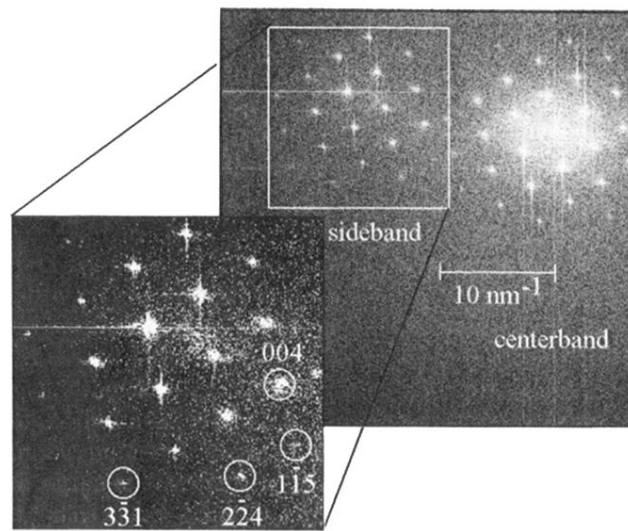


FIG. 6. Spectrum of image wave reconstructed from a Si [110] hologram containing information up to 0.104 nm. The  $3\bar{3}1$ ,  $2\bar{2}4$ , and  $1\bar{1}5$  reflections present correspond to lateral information of 0.124, 0.111, and 0.104 nm, respectively.